



# Different TiO<sub>2</sub> Phases (Degussa/Anatase) Modified Cross-Linked Chitosan Composite for the Removal of Reactive Red 4 Dye: Box–Behnken Design

Ahmed Saud Abdulhameed<sup>1,2</sup> · Ali H. Jawad<sup>3</sup> · Sivakumar Vigneshwaran<sup>4</sup> · Zeid A. ALOthman<sup>5</sup> · Zaher Mundher Yaseen<sup>6,7</sup>

Accepted: 25 August 2022 / Published online: 12 September 2022

© The Author(s), under exclusive licence to Springer Science+Business Media, LLC, part of Springer Nature 2022

## Abstract

The present work targets to develop the cross-linked chitosan composite with different TiO<sub>2</sub> phases (Degussa/Anatase) to attain two adsorbents namely cross-linked chitosan-epichlorohydrin/TiO<sub>2</sub>-Degussa (CS-ECH/TiO<sub>2</sub>-D) and cross-linked chitosan-epichlorohydrin/TiO<sub>2</sub>-Anatase (CS-ECH/TiO<sub>2</sub>-A). The physicochemical characteristics including crystalline nature, specific surface area, functional groups, surface morphology, and thermal stability of the prepared composites were identified by X-ray diffraction (XRD), Brunauer–Emmett–Teller (BET), Fourier transform infrared (FTIR), scanning electron microscope (SEM), and thermogravimetric and derivative thermogravimetric analyses (TGA-DTG), respectively. Response surface methodology combined with Box–Behnken design (RSM-BBD) was used to explore multivariate modeling and optimization of reactive red 4 (RR4) dye removal on CS-ECH/TiO<sub>2</sub>-D and CS-ECH/TiO<sub>2</sub>-A based on the related factors including A: adsorbent dose (0.5–1.5 g/100 mL), B: pH (4–10), and C: time (30–90 min). RR4 dye removal was 94.6 and 87.5% for CS-ECH/TiO<sub>2</sub>-D and CS-ECH/TiO<sub>2</sub>-A, respectively. The adsorption of RR4 molecules on the surface of CS-ECH/TiO<sub>2</sub>-(D/A) was constructed by many interactions e.g. electrostatic forces, n–π stacking, and H-bonding. The findings revealed that the biomaterials developed could be viable and convenient potential adsorbents for capturing azo dyes from polluted effluents.

**Keywords** Chitosan · TiO<sub>2</sub> · Box–Behnken design · Reactive red 4 dye · Adsorption mechanism

✉ Ali H. Jawad  
ali288@uitm.edu.my; ahjm72@gmail.com

- <sup>1</sup> Department of Medical Instrumentation Engineering, Al-Mansour University College, Baghdad, Iraq
- <sup>2</sup> College of Engineering, University of Warith Al-Anbiyaa, Karbala, Iraq
- <sup>3</sup> Faculty of Applied Sciences, Universiti Teknologi MARA, 40450 Shah Alam, Selangor, Malaysia
- <sup>4</sup> Environmental System Laboratory, Department of Civil Engineering, Kyung Hee University-Global Campus, 1732 Deogyong-daero, Giheung-Gu, Yongin-Si, GyeonggiDo 16705, Republic of Korea
- <sup>5</sup> Chemistry Department, College of Science, King Saud University, Riyadh 11451, Saudi Arabia
- <sup>6</sup> UniSQ's Advanced Data Analytics Research Group, School of Mathematics Physics and Computing, University of Southern Queensland, Toowoomba, QLD 4300, Australia
- <sup>7</sup> New Era and Development in Civil Engineering Research Group, Scientific Research Center, Al-Ayen University, Thi-Qar, Nasiriyah 64001, Iraq

## Introduction

The enormous manufacturing activity and urban development have significantly increased the wastewaters polluted with textile dyes, heavy metals, and medicines, resulting in vast volumes of contaminated water [1]. One of the anionic and reactive azo dyes (containing one or more azo (–N=N–) groups with aromatic rings and sulfonate groups) used in the printing, textile, and dyeing of cellulose fibers industries is Reactive Red 4 (RR4) dye, also recognized as Cibracron Brilliant Red (CBR) dye [2]. Azo dyes are hazardous to living beings, especially aquatic life, and can even cause mutations [2]. The release of untreated effluents containing azo dyes into water bodies poses a serious threat to freshwater ecosystems and people due to its carcinogenic potential, non-biodegradability, and toxic effects [3]. Because of the serious consequences of increasing contamination of water with textile dyes, it is critical to remediate polluted water before it is released into rivers and streams. Various technologies for removing reactive

dyes from wastewaters have been extensively researched, comprising membrane nanofiltration [4], electrochemical oxidation [5], microbiological decolorization [6], photocatalytic degradation [7], and adsorption [8]. Adsorption is one of the most common and widely used procedures for the remediation of organic pollutants due to its efficiency, simplicity of design, environmentally friendly nature, flexibility, economic feasibility, and superior selectivity [9].

Chitosan (CS) is a linear natural polymer composed of 2-amino-2-deoxy-D-glucopyranose units produced from the chitin existent in the exoskeleton of crustaceans like shrimps and crabs [10]. CS has a number of distinct characteristics including biodegradability, chemical reactivity, natural abundance, adsorption capacity, nontoxicity, antibacterial activity, and biocompatibility [11]. The structure of CS is distinguished by the existence of active adsorption sites (amino and hydroxyl groups), making it a preferable adsorbent in wastewater remediation methods [12, 13]. Recently, CS composites have been widely researched as an effective adsorbent for the removal of toxic industrial dyes like methyl orange [14], amido black 10B and methylene blue [15], acid blue-113 and rhodamine B [16], brilliant green [17], eriochrome black T [18], and amaranth dyes [19].

However, CS has drawbacks in its application as an adsorbent in adsorption strategies, such as low mechanical characteristics, pH-dependence (solubilized or gelatinous form in acidic media), and limited surface area [20]. Several approaches including crosslinking [21], composition [22], and grafting [23] have been proposed to address these restrictions and strengthen the physicochemical characteristics of the CS. Typically, crosslinking techniques are commonly employed to strengthen the chemical stability of CS as an adsorbent in acidic environments and lowering hydrophobicity [24]. Cross-linked CS has been typically prepared using a variety of cross-linker chemicals, including glyoxal, glutaraldehyde, benzil, and ethylene glycol diglycidyl ether (EGDE). The  $-NH_2$  groups in the CS backbone are blocked by these cross-linker agents, which is their main drawback. Epichlorohydrin (ECH) works well as a mono-functional cross-linking agent since it won't react to amino groups in CS biopolymer, which serve as active adsorption sites for acidic dyes, while ECH binds covalently with hydroxyl groups of CS [25].

The composition of metal oxides such as titanium dioxide ( $TiO_2$ ) and magnesium oxide (MgO) with the polymeric network of CS has been widely implemented for increasing the physicochemical characteristics of CS i.e. adsorption capacity, mechanical performance, porosity, and surface area [26, 27].  $TiO_2$  possesses numerous desirable characteristics, including large surface area, chemical resistance in acidic and basic solutions conditions, insolubility in water, and environmental friendliness [28]. Currently, CS- $TiO_2$

biomaterials are extensively and successfully used in a variety of applications such as food packaging [29], wastewater treatment [30], biosensors [31], and antibacterial [32].

Titanium dioxide exists in different phases and particle sizes, which affect the surface area property and porosity. Thus, the aim of this study is to investigate the role of different  $TiO_2$  phases (Degussa/Anatase) on the adsorptive behavior of the cross-linked chitosan composite for removal of reactive red 4 dye (RR4). To achieve this aim, two new composite adsorbents namely cross-linked chitosan-epichlorohydrin/ $TiO_2$ -Degussa (CS-ECH/ $TiO_2$ -D) and cross-linked chitosan-epichlorohydrin/ $TiO_2$ -Anatase (CS-ECH/ $TiO_2$ -A) were prepared and their adsorptive behavior towards RR4 removal was compared. Furthermore, response surface methodology (RSM) integrated with Box–Behnken design (BBD) was appointed for modeling and optimization of the RR4 dye removal by CS-ECH/ $TiO_2$ -D and CS-ECH/ $TiO_2$ -A in the light of input factors involving adsorbent dosage, initial pH, and time. A realistic mechanism has been proposed for RR4 dye adsorption on the CS-ECH/ $TiO_2$ -(D/A) surfaces.

## Materials and Methods

### Materials

Chitosan (CS) flakes (75% deacetylation), epichlorohydrin ( $\geq 98\%$  [w/v]),  $TiO_2$  Degussa P-25 (nanoparticle size = 21 nm), and  $TiO_2$  Anatase (particle size  $\leq 150 \mu m$ ) were supplied by Sigma-Aldrich. The RR4 dye (chemical formula:  $C_{32}H_{23}ClN_8Na_4O_{14}S_4$ ; M.W = 995.23 g/mol;  $\lambda_{max} = 517$  nm, Sigma-Aldrich) stock solution (1000 mg/L) was prepared and diluted as needed for adsorption tests. R&M Chemicals provided chemical compounds like sodium hydroxide (NaOH) pellets, hydrochloric acid (HCl), and sodium chloride (NaCl) powder. The RR4 dye solutions and adsorption experiments were generated with deionized water.

### Preparation of CS-ECH/ $TiO_2$ -(D/A)

A beaker containing 50 mL of acetic acid solution (5% v/v) was loaded with 1 g of CS flakes and 1 g of  $TiO_2$ -(D/A) and gently stirred for 24 h at room temperature. A syringe needle (10 mL) was used to inject the resulting solution into 1000 mL of sodium hydroxide (0.5 M), and CS- $TiO_2$ -(D/A) beads were immediately generated. To eliminate the NaOH residue, distilled water was used to wash the CS- $TiO_2$ -(D/A) beads. The CS- $TiO_2$ -(D/A) beads were subjected to the crosslinking reaction stage by adding 2% ECH (90 mL) and agitating in a water bath for 2 h at 40 °C. The CS-ECH/ $TiO_2$ -(D/A) beads were then washed, dried in an oven for

an entire night at 80 °C, ground to consistent particle size (about 250 µm), and stored in a closed container for subsequent use.

## Characterization

The Brunauer Emmet Teller (BET) technique (Micromeritics ASAP 2060) was conducted to determine the surface parameters (e.g., specific surface area and pore volume) of the biomaterials including CS-ECH/TiO<sub>2</sub>-D and CS-ECH/TiO<sub>2</sub>-A using N<sub>2</sub> adsorption–desorption isotherms at temperature 77 K. A scanning electron microscope (SEM, Zeiss Supra 40 VP) was used to characterize the morphological features of CS-ECH/TiO<sub>2</sub>-D and CS-ECH/TiO<sub>2</sub>-A before and after RR4 dye adsorption. A gold-coating apparatus was used to coat the samples with gold after mounting them on stubs, and the SEM analysis was carried out at 15.0 keV to obtain high-resolution SEM images. A PANalytical X'Pert PRO diffractometer was used to acquire X-ray diffraction (XRD, Cu Kα radiation (λ = 1.54 Å), 40 kV, 20 mA) with patterns of CS-ECH/TiO<sub>2</sub>-D and CS-ECH/TiO<sub>2</sub>-A across the 2-theta (5° to 90°) range. At wavenumbers range between 4000 and 450 cm<sup>-1</sup>, Fourier transform infrared (FTIR, Perkin-Elmer, Spectrum RX I) spectroscopy was used to define the primary functional groups of the CS-ECH/TiO<sub>2</sub>-D and CS-ECH/TiO<sub>2</sub>-A before and after RR4 dye adsorption. KBr pellets were used to prepare the samples for FTIR analysis. Thermal Analyzer (NETZSCH STA 449 F5 Jupiter®) was utilized to obtain the thermogravimetric and derivative thermogravimetric (TGA-DTG) curves of CS-ECH/TiO<sub>2</sub>-D and CS-ECH/TiO<sub>2</sub>-A. Thermograms were obtained within the range of 30 °C/(10.0 K/min)/1200 °C under N<sub>2</sub> atmosphere. A zero point of charge (pH<sub>pzc</sub>) procedure was used to specify the charge on the CS-ECH/TiO<sub>2</sub>-D and CS-ECH/TiO<sub>2</sub>-A surfaces [33].

## Statistical Optimization Methodology

RSM-BBD was utilized to optimize and analyze the three variables (adsorbent dose, pH, and time) which possess the greatest impact on RR4 dye adsorption by CS-ECH/TiO<sub>2</sub>-D and CS-ECH/TiO<sub>2</sub>-A. The Design Expert (version 13, Stat-Ease, Minneapolis, USA) software was used to design removal tests and statistically assess the results. Table 1 depicts the ranges of the investigated inputs along with their codes. The limits of each of the variables tested in the experimental design were defined as per premonitory tests. Based on this, a second quadratic expression was used to find out the correlation between the specified inputs and the yields labeled RR4 removal by CS-ECH/TiO<sub>2</sub>-D and RR4 removal

**Table 1** Codes and actual variables and their levels in BBD

Codes	Variables	Level 1 (-1)	Level 2 (0)	Level 3 (+1)
A	Adsorbent dose (g)	0.5	1	1.5
B	pH	4	7	10
C	Time (min)	30	60	90

by CS-ECH/TiO<sub>2</sub>-A. Equation 1 contains the mathematical formula for the 2nd quadratic polynomial model.

$$Y = \beta_0 + \sum \beta_i X_i + \sum \beta_{ii} X_i^2 + \sum \sum \beta_{ij} X_i X_j \quad (1)$$

where  $Y$  denotes the predicted outputs;  $X_i$  and  $X_j$  denote independent removal factors. The intercept, straight, quadratic influence, and association affect regression coefficients are denoted by  $\beta_0$ ,  $\beta_i$ ,  $\beta_{ii}$ , and  $\beta_{ij}$ , respectively. Hence, seventeen tests derived from the BBD model were performed to illustrate and evaluate the effect of various input factors [A: adsorbent dose (0.5–1.5 g), B: pH (4–10), and C: time (30–90 min)] on the removal of RR4 dye. Table 2 illustrates the limits of the investigated factors as well as the corresponding measured responses (RR4 removal by CS-ECH/TiO<sub>2</sub>-D and RR4 removal by CS-ECH/TiO<sub>2</sub>-A). The RR4 dye removal tests started with pouring a specific mass of adsorbent into a set of 250 mL Erlenmeyer flasks having 100 mL of RR4 dye solution. The mixtures were incubated in a shaking water bath (WNB7-45, Memmert) and agitated at a regular rate of 80 r.p.m for a specific period of time. The mixtures were then purified via a syringe filter (0.45 µm) to produce adsorbent-free solutions. The residual concentration in RR4 dye solutions was spectrophotometrically measured at λ<sub>max</sub> 517 nm using UV–Vis (HACH DR 2800). The removal efficiency ( $R$ , %) of RR4 dye was computed by applying the following formula (2):

$$R\% = \frac{(C_o - C_e)}{C_o} \times 100 \quad (2)$$

where in  $C_o$  and  $C_e$  are the starting and equilibrium concentrations (mg/L) of adsorbate (RR4 dye).

## Results and Discussion

### Characterization of the Prepared Composites

#### Specific Surface Area Analysis

Textural characteristics i.e. specific surface area, total pore volume, and mean pore diameter of CS-ECH/TiO<sub>2</sub>-D and CS-ECH/TiO<sub>2</sub>-A are tabulated in Table 3. As shown in Table 3, the specific surface area of CS-ECH/

**Table 2** The 3-variables BBD matrix and experimental data for RR4 removal (%) by CS-ECH/TiO<sub>2</sub>-D and RR4 removal (%) by CS-ECH/TiO<sub>2</sub>-A

Run	A: Adsorbent dose (g)	B: pH	C: Time (min)	RR4 removal (%) by CS-ECH/TiO <sub>2</sub> -D	RR4 removal (%) by CS-ECH/TiO <sub>2</sub> -A
1	0.5	4	60	50.9	34.3
2	1.5	4	60	94.6	87.5
3	0.5	10	60	36.2	24.3
4	1.5	10	60	68.8	49.9
5	0.5	7	30	39.6	24.6
6	1.5	7	30	65.9	52.6
7	0.5	7	90	49.2	37.8
8	1.5	7	90	87.6	82.1
9	1	4	30	62.3	51.3
10	1	10	30	41.7	20.3
11	1	4	90	82.1	66.2
12	1	10	90	53.2	42.4
13	1	7	60	69.4	52.9
14	1	7	60	69	53.8
15	1	7	60	68.1	54
16	1	7	60	67	53.9
17	1	7	60	69.1	54.3

**Table 3** The textile properties of CS-ECH/TiO<sub>2</sub>-D and CS-ECH/TiO<sub>2</sub>-A

Analysis	CS-ECH/TiO <sub>2</sub> -D	CS-ECH/TiO <sub>2</sub> -A
BET surface area (m <sup>2</sup> /g)	28.08	10.10
V <sub>m</sub> (cm <sup>3</sup> /g)	6.45	2.32
Total pore volume (cm <sup>3</sup> /g)	0.299	0.112
Mean pore diameter (nm)	42.67	44.32

TiO<sub>2</sub>-D (28.08 m<sup>2</sup>/g) was larger than that of CS-ECH/TiO<sub>2</sub>-A (10.10 m<sup>2</sup>/g). This finding is associated with the fact that the particles of TiO<sub>2</sub> (Degussa) are nanoscale, and thus this feature is reflected on the specific surface area of the CS-ECH/TiO<sub>2</sub>-D. This difference is impacted positively in the adsorptive removal of the generated biomaterials, as the RR4 dye removal (see Table 2) was 94.6% for CS-ECH/TiO<sub>2</sub>-D and 87.5% for CS-ECH/TiO<sub>2</sub>-A. In addition, the mean pore diameters of CS-ECH/TiO<sub>2</sub>-D and CS-ECH/TiO<sub>2</sub>-A are 42.67 nm and 44.32 nm, respectively. As per IUPAC, the structure of CS-ECH/TiO<sub>2</sub>-D and CS-ECH/TiO<sub>2</sub>-A have a mesoporous nature (mean pore diameter = 2–50 nm) [34]. The N<sub>2</sub> adsorption–desorption isotherm plots and the BJH pore diameter distributions (inset) of CS-ECH/TiO<sub>2</sub>-D and CS-ECH/TiO<sub>2</sub>-A are included in Fig. 1a, b. As per the IUPAC classification, the isotherms shown in Fig. 1a, b exhibit a type IV isotherm with an obvious hysteresis loop, indicating the existence of mesopores in CS-ECH/TiO<sub>2</sub>-D and CS-ECH/TiO<sub>2</sub>-A [35]. Furthermore, it is obvious that the hysteresis

loop approaches relative pressure ( $P/P_0 = 1$ ), confirming the presence of macropores in CS-ECH/TiO<sub>2</sub>-D and CS-ECH/TiO<sub>2</sub>-A [35]. Such findings were consistent with the BJH plots of CS-ECH/TiO<sub>2</sub>-D and CS-ECH/TiO<sub>2</sub>-A (see inserted Figs. in Fig. 2), which revealed that the CS-ECH/TiO<sub>2</sub>-D and CS-ECH/TiO<sub>2</sub>-A exhibited a broad pore diameter range involving the mesoporous and macroporous domains.

### XRD Analysis

The XRD technique was used to assess the nature of the CS-ECH/TiO<sub>2</sub>-D and CS-ECH/TiO<sub>2</sub>-A forms, as well as to characterize the crystalline phase of the produced CS-ECH/TiO<sub>2</sub>-D and CS-ECH/TiO<sub>2</sub>-A structures. The XRD patterns of the CS-ECH/TiO<sub>2</sub>-D and CS-ECH/TiO<sub>2</sub>-A are presented in Fig. 2. The characteristic peaks located at  $2\theta = 10.5^\circ$  and  $20^\circ$  are attributed to (020) and (110) reflections of CS, respectively [36]. The XRD examination of CS-ECH/TiO<sub>2</sub>-D and CS-ECH/TiO<sub>2</sub>-A revealed a number of distinct and sharp peaks at  $25.15^\circ$ ,  $37.89^\circ$ ,  $47.95^\circ$ ,  $54.25^\circ$ ,  $55.01^\circ$ ,  $63.82^\circ$ , and  $68.90^\circ$ , corresponding to the crystal planes (101), (004), (200), (105), (211), (204), and (116) of TiO<sub>2</sub> [37]. These findings show that there is a significant interaction between crystalline TiO<sub>2</sub> and CS, which leads to the formation of a crystal region in the CS matrix. This demonstrates that the CS-ECH/TiO<sub>2</sub>-D and CS-ECH/TiO<sub>2</sub>-A biomaterials were successfully formed. The crystalline phase of CS-ECH/TiO<sub>2</sub>-D and CS-ECH/

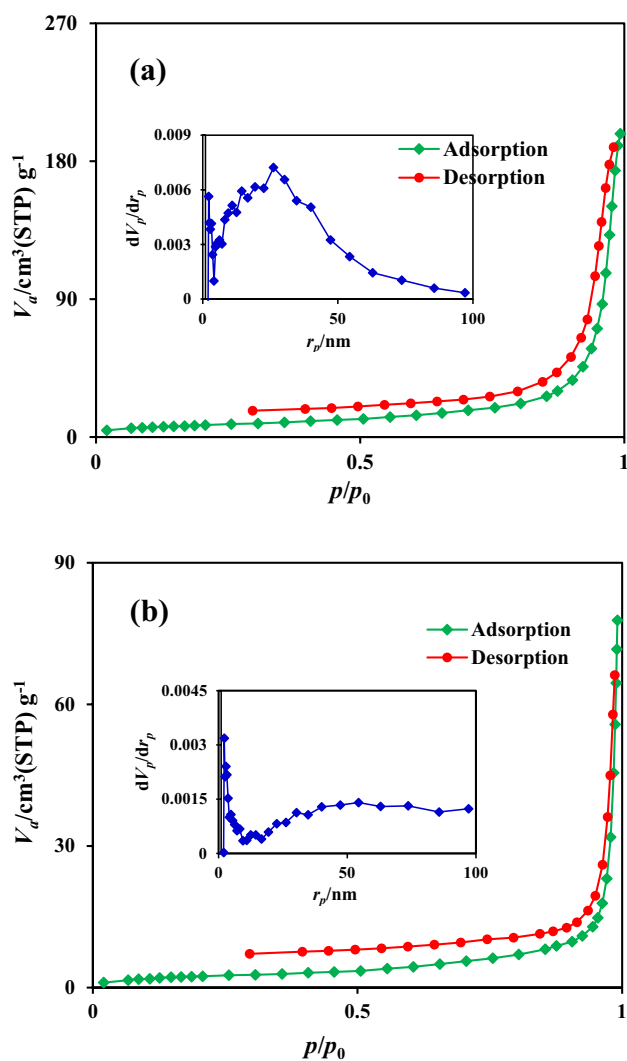


**Fig. 1** The N<sub>2</sub> adsorption–desorption isotherm plots of **a** CS-ECH/TiO<sub>2</sub>-D and **b** CS-ECH/TiO<sub>2</sub>-A

TiO<sub>2</sub>-A is also associated with intramolecular and intermolecular hydrogen bonding [38].

### TGA-DTG Analysis

The thermal properties of CS-ECH/TiO<sub>2</sub>-D and CS-ECH/TiO<sub>2</sub>-A were evaluated using TGA-DTG analysis. Figure 3 illustrates the TGA-DTG graphs of (a) CS-ECH/TiO<sub>2</sub>-D and (b) CS-ECH/TiO<sub>2</sub>-A. The TGA-DTG graphs of CS-ECH/TiO<sub>2</sub>-D and CS-ECH/TiO<sub>2</sub>-A show that two stages of breakdown occurred across a broad range of temperatures. The initial step of degradation for CS-ECH/TiO<sub>2</sub>-D and CS-ECH/TiO<sub>2</sub>-A proceeded at temperatures ranging from 27 to 200 °C and 27.1 to 209.4 °C, respectively, with weight losses of 2.17 mg (16.3%) for CS-ECH/TiO<sub>2</sub>-D and 2.7 mg

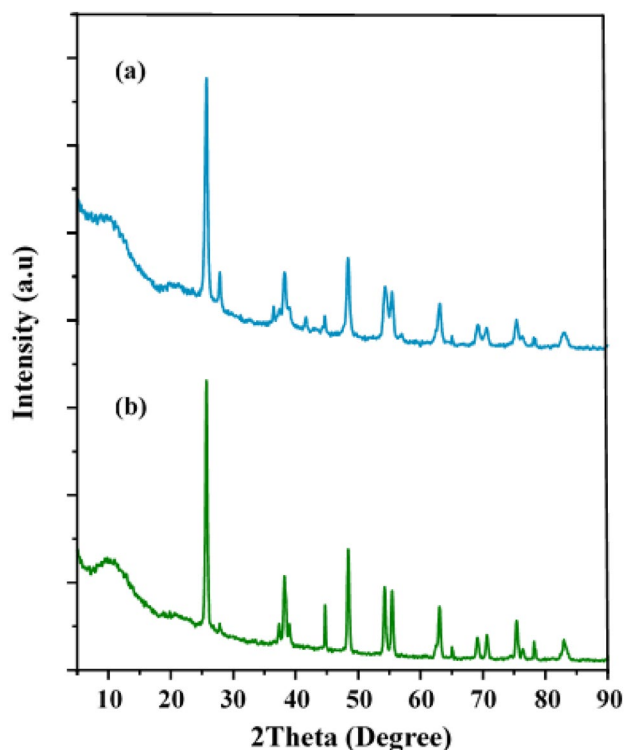


**Fig. 2** XRD patterns of **a** CS-ECH/TiO<sub>2</sub>-D and **b** CS-ECH/TiO<sub>2</sub>-A

(18.88%) for CS-ECH/TiO<sub>2</sub>-A. The weight loss of CS-ECH/TiO<sub>2</sub>-D and CS-ECH/TiO<sub>2</sub>-A during the initial step of the analysis is related to the loss of water bonded or held in the material, which is likely related to the hydrophilic nature of CS [39]. The 2nd step of degradation for CS-ECH/TiO<sub>2</sub>-D and CS-ECH/TiO<sub>2</sub>-A happened at temperatures ranging from 201 to 672 °C and 210 to 672 °C, respectively, with a mass loss of 8.1 mg (60.03%) for CS-ECH/TiO<sub>2</sub>-D and 8.8 mg (60.8%) for CS-ECH/TiO<sub>2</sub>-A. The major reduction in mass of CS-ECH/TiO<sub>2</sub>-D and CS-ECH/TiO<sub>2</sub>-A at the second phase could be attributed to complex dehydration of polymeric rings, deacetylation of acetyl units, polymerization, and decomposition of the linking between Ti–O network and the CS-ECH/TiO<sub>2</sub>-(D/A) composite [37, 40]. In both CS-ECH/TiO<sub>2</sub>-D and CS-ECH/TiO<sub>2</sub>-A at 672 °C, the mass of residual is linked to the titanium content, and the primary residual component is TiO<sub>2</sub> [40]. At 200–600 °C, the pure CS showed a quick weight loss and the CS totally decomposed when the temperature reached ~650 °C. It may be stated that TiO<sub>2</sub> improved the thermal stability of CS-ECH/TiO<sub>2</sub>-D and CS-ECH/TiO<sub>2</sub>-A biomaterials [40, 41]. Briefly, the overall weight loss of CS-ECH/TiO<sub>2</sub>-D and CS-ECH/TiO<sub>2</sub>-A at 672 °C was approximately 76.1% and 79.6%, respectively, owing to CS biopolymer decomposition, which correlates to previously published works [37, 40].

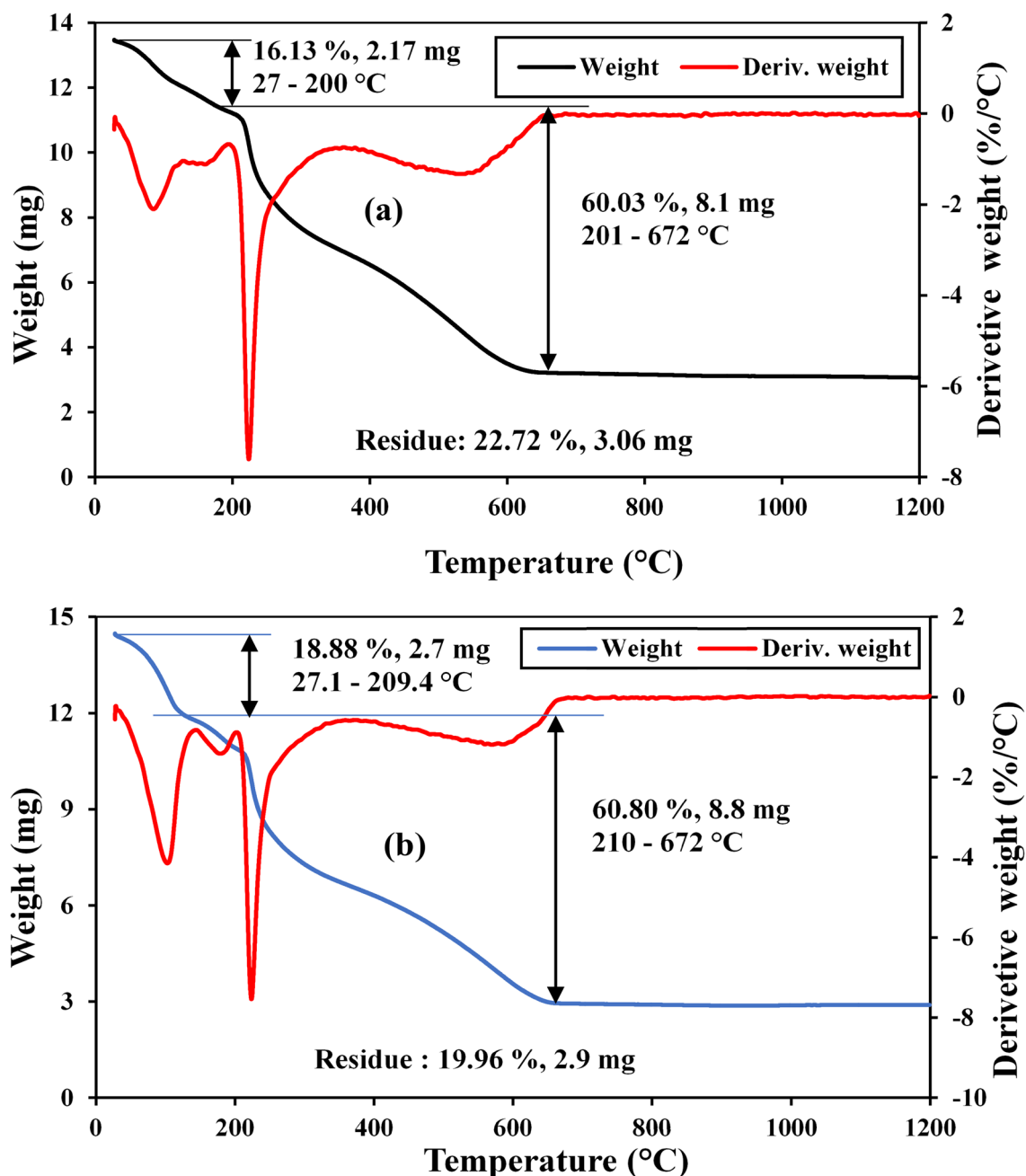
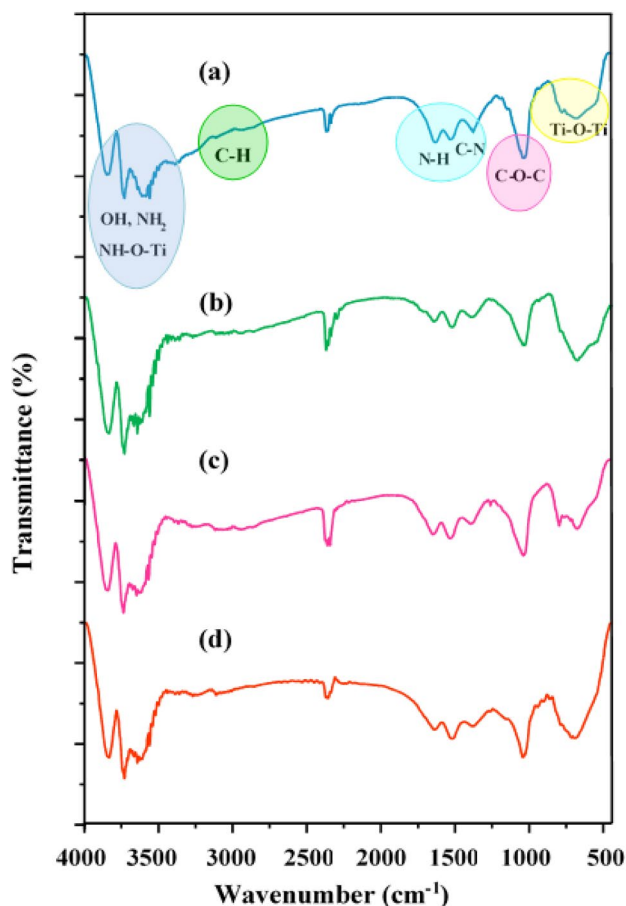


Fig. 3 TGA-DTG graphs of a CS-ECH/TiO<sub>2</sub>-D and b CS-ECH/TiO<sub>2</sub>-A

### FTIR Analysis

The FTIR approach was used to reveal one of the unique properties of CS-ECH/TiO<sub>2</sub>-D and CS-ECH/TiO<sub>2</sub>-A, which is characterizing the type of functional groups existent on the surface of the CS-ECH/TiO<sub>2</sub>-D and CS-ECH/TiO<sub>2</sub>-A and thus estimating the capacity of CS-ECH/TiO<sub>2</sub>-D and CS-ECH/TiO<sub>2</sub>-A to adsorb anionic RR4 dye. Figure 4 shows the FTIR spectra of CS-ECH/TiO<sub>2</sub>-D and CS-ECH/TiO<sub>2</sub>-A before and after RR4 dye adsorption. The structures of

CS-ECH/TiO<sub>2</sub>-D and CS-ECH/TiO<sub>2</sub>-A have prominent bands positioned at 3450–3775 cm<sup>-1</sup>, as seen in the FTIR spectra of CS-ECH/TiO<sub>2</sub>-D and CS-ECH/TiO<sub>2</sub>-A, which are connected to the stretching mode of the O–H and N–H groups of CS as well as electrostatic interaction of NH–O–Ti [42]. The peak at 2930 cm<sup>-1</sup> is related to the asymmetrical stretching mode of the C–H [42]. The peaks positioned at 1673 cm<sup>-1</sup> and 1538 cm<sup>-1</sup> are linked with the in-plane N–H bending vibration and –CH<sub>2</sub> bending, respectively [37]. The peaks located at 1378 cm<sup>-1</sup> and 1029 cm<sup>-1</sup> are attributed to the C–N



**Fig. 4** FTIR spectra of (a) CS-ECH/TiO<sub>2</sub>-D, (b) CS-ECH/TiO<sub>2</sub>-A, (c) CS-ECH/TiO<sub>2</sub>-D after adsorption of RR4 dye, and (d) CS-ECH/TiO<sub>2</sub>-A after RR4 dye adsorption

stretching and C–O–C stretching vibrations, respectively [43]. The band located between 600 cm<sup>-1</sup> and 900 cm<sup>-1</sup> is attributed to the vibrations of the asymmetric stretching mode of the Ti–O and Ti–O–Ti bond, indicating the existence of TiO<sub>2</sub> particles in the produced composites [42]. The FTIR spectra following RR4 adsorption on the surface of CS-ECH/TiO<sub>2</sub>-D (Fig. 4c) and CS-ECH/TiO<sub>2</sub>-A (Fig. 4d) demonstrate that they have largely similar profiles to CS-ECH/TiO<sub>2</sub>-D and CS-ECH/TiO<sub>2</sub>-A with variations in some bands, indicating that the primary functional groups of CS-ECH/TiO<sub>2</sub>-D and CS-ECH/TiO<sub>2</sub>-A are involved in the RR4 dye adsorption.

### SEM Analysis

SEM analysis was used to investigate the morphological properties of the CS-ECH/TiO<sub>2</sub>-D and CS-ECH/TiO<sub>2</sub>-A surfaces before and after adsorption of RR4 molecules. SEM images of (a) CS-ECH/TiO<sub>2</sub>-D, (b) CS-ECH/TiO<sub>2</sub>-A, (c)

CS-ECH/TiO<sub>2</sub>-D after adsorption of RR4, and (d) CS-ECH/TiO<sub>2</sub>-A after adsorption of RR4 are given in Fig. 5. The morphologies of CS-ECH/TiO<sub>2</sub>-D (a) and CS-ECH/TiO<sub>2</sub>-A (b) biomaterials appear to be heterogeneous and amorphous, with the presence of holes, fractures, and crevasses. The outer surface of CS-ECH/TiO<sub>2</sub>-D after RR4 adsorption is generally smooth and has a regular structure with an obvious lack of pores, indicating that the surface of CS-ECH/TiO<sub>2</sub>-D was uniformly covered with RR4 particles, as shown in Fig. 5c. Regarding the adsorption of RR4 on the surface of CS-ECH/TiO<sub>2</sub>-A (Fig. 5d), the surface of CS-ECH/TiO<sub>2</sub>-A has changed to be slightly compact, with a considerable reduction in porosity and cracks, demonstrating the loading of RR4 dye on the CS-ECH/TiO<sub>2</sub>-A surface.

### BBD Model Analysis

ANOVA is a core method for analyzing the applicability of the employed BBD model, namely RR4 removal by CS-ECH/TiO<sub>2</sub>-D and CS-ECH/TiO<sub>2</sub>-A, along with determining the impactful codes and validity of the collected data belonging to the BBD model. The ANOVA characteristics for RR4 removal by CS-ECH/TiO<sub>2</sub>-D and CS-ECH/TiO<sub>2</sub>-A are tabulated in Table 4. The data recorded in Table 4 show that the applied models i.e. RR4 removal by CS-ECH/TiO<sub>2</sub>-D and RR4 removal by CS-ECH/TiO<sub>2</sub>-A are favorable, where F-values are 42.95 (p-value 0.0001) and 77.91 (p-value 0.0007) for RR4 removal by CS-ECH/TiO<sub>2</sub>-D and RR4 removal by CS-ECH/TiO<sub>2</sub>-A, respectively [44]. The coefficients of determination (*R*<sup>2</sup>) for RR4 removal utilizing CS-ECH/TiO<sub>2</sub>-D and CS-ECH/TiO<sub>2</sub>-A appear to be 0.99 and 0.99, respectively. This result reveals that the practical and calculated outcomes are highly compatible with each other, and the selected BBD was effective in optimizing the RR4 dye removal. [45]. Statistically, inputs with p-values *p* < 0.05 are frequently known as statistically relevant in terms of RR4 removal by CS-ECH/TiO<sub>2</sub>-D and RR4 removal by CS-ECH/TiO<sub>2</sub>-A [46]. Thus, the model terms of RR4 removal by CS-ECH/TiO<sub>2</sub>-D, comprising A, B, C, AB, AC, A<sup>2</sup>, B<sup>2</sup>, and C<sup>2</sup>, were identified as relevant model terms. On the other side, the model terms of RR4 removal by CS-ECH/TiO<sub>2</sub>-A, comprising A, B, C, AB, AC, B<sup>2</sup>, and C<sup>2</sup> were identified as relevant model terms. As expressed in Eq. 3 and Eq. 4, the 2nd polynomial function representations contain the outputs (RR4 removal by CS-ECH/TiO<sub>2</sub>-D and RR4 removal by CS-ECH/TiO<sub>2</sub>-A) and analyzed inputs after fitting has been attained.

$$\begin{aligned} \text{RR4 removal (\%)} & \text{ by CS - ECH/TiO}_2 \text{ - D} \\ & = +68.52 + 17.62A - 11.25B + 7.82C - 2.78AB \\ & \quad + 3.02AC - 2.57A^2 - 3.32B^2 - 5.37C^2 \end{aligned} \quad (3)$$

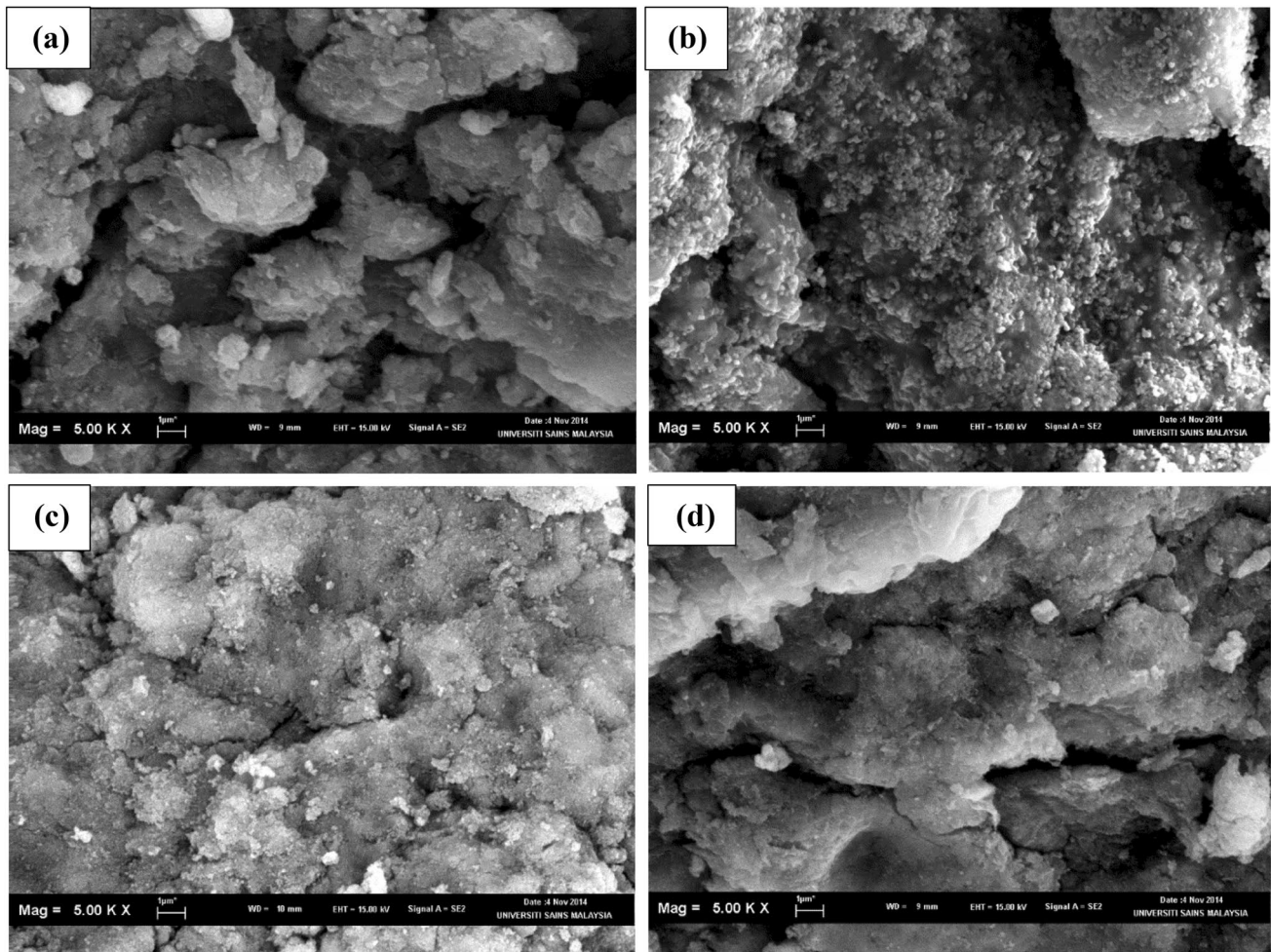


**Fig. 5** SEM images **a** CS-ECH/TiO<sub>2</sub>-D, **b** CS-ECH/TiO<sub>2</sub>-A, **c** CS-ECH/TiO<sub>2</sub>-D after adsorption of RR4, and **d** CS-ECH/TiO<sub>2</sub>-A after adsorption of RR4

**Table 4** ANOVA of RR4 removal (%) by CS-ECH/TiO<sub>2</sub>-D and RR4 removal (%) by CS-ECH/TiO<sub>2</sub>-A

Source	RR4 removal (%) by CS-ECH/TiO <sub>2</sub> -D					RR4 removal (%) by CS-ECH/TiO <sub>2</sub> -A				
	Sum of Squares	df	Mean Square	F-value	p-value	Sum of Squares	df	Mean Square	F-value	p-value
Model	4288.05	9	476.45	108.38	<0.0001	5400.43	9	600.05	248.09	<0.0001
A-Adsorbent dose	2485.13	1	2485.13	565.30	<0.0001	2853.90	1	2853.90	1179.96	<0.0001
B-pH	1012.50	1	1012.50	230.32	<0.0001	1310.72	1	1310.72	541.92	<0.0001
C-Time	489.84	1	489.84	111.43	<0.0001	794.01	1	794.01	328.29	<0.0001
AB	30.80	1	30.80	7.01	0.0331	190.44	1	190.44	78.74	<0.0001
AC	36.60	1	36.60	8.33	0.0235	66.42	1	66.42	27.46	0.0012
BC	17.22	1	17.22	3.92	0.0883	12.96	1	12.96	5.36	0.0538
A <sup>2</sup>	27.86	1	27.86	6.34	0.0400	0.3242	1	0.3242	0.1341	0.7251
B <sup>2</sup>	46.48	1	46.48	10.57	0.0140	85.36	1	85.36	35.29	0.0006
C <sup>2</sup>	121.53	1	121.53	27.65	0.0012	75.25	1	75.25	31.11	0.0008
Residual	30.77	7	4.40			16.93	7	2.42		
Pure error	3.83	4	0.9570			1.11	4	0.2770		
Cor total	4318.82	16				5417.36	16			

RR4 removal (%) by CS – ECH/TiO<sub>2</sub> – A

$$= +53.78 + 18.89A - 12.8B + 9.96C - 6.90AB \quad (4) \\ + 4.07AC - 4.50B^2 - 4.23C^2$$

Additionally, the BBD diagrams like the normal probability of residuals and the plot of the relationship between the predicted and actual values are employed to validate the developed models including RR4 removal by CS-ECH/TiO<sub>2</sub>-D and RR4 removal by CS-ECH/TiO<sub>2</sub>-A. The diagrams of the experimental and theoretical values of RR4 removal by CS-ECH/TiO<sub>2</sub>-D and RR4 removal by CS-ECH/TiO<sub>2</sub>-A are exhibited in Fig. 6c and d, respectively. From Fig. 6c and d, it is apparent that there is

include RR4 removal by CS-ECH/TiO<sub>2</sub>-D and RR4 removal by CS-ECH/TiO<sub>2</sub>-A are given in Fig. 6a and b, respectively. The points in Fig. 6a and b appear to be neatly connected with a single line, showing that the points are consistently and precisely disseminated, and the residuals are independently distributed [47]. These results also imply that the generated models can simulate the removal of RR4 by CS-ECH/TiO<sub>2</sub>-D and CS-ECH/TiO<sub>2</sub>-A. The diagrams of the experimental and theoretical values of RR4 removal by CS-ECH/TiO<sub>2</sub>-D and RR4 removal by CS-ECH/TiO<sub>2</sub>-A are exhibited in Fig. 6c and d, respectively. From Fig. 6c and d, it is apparent that there is

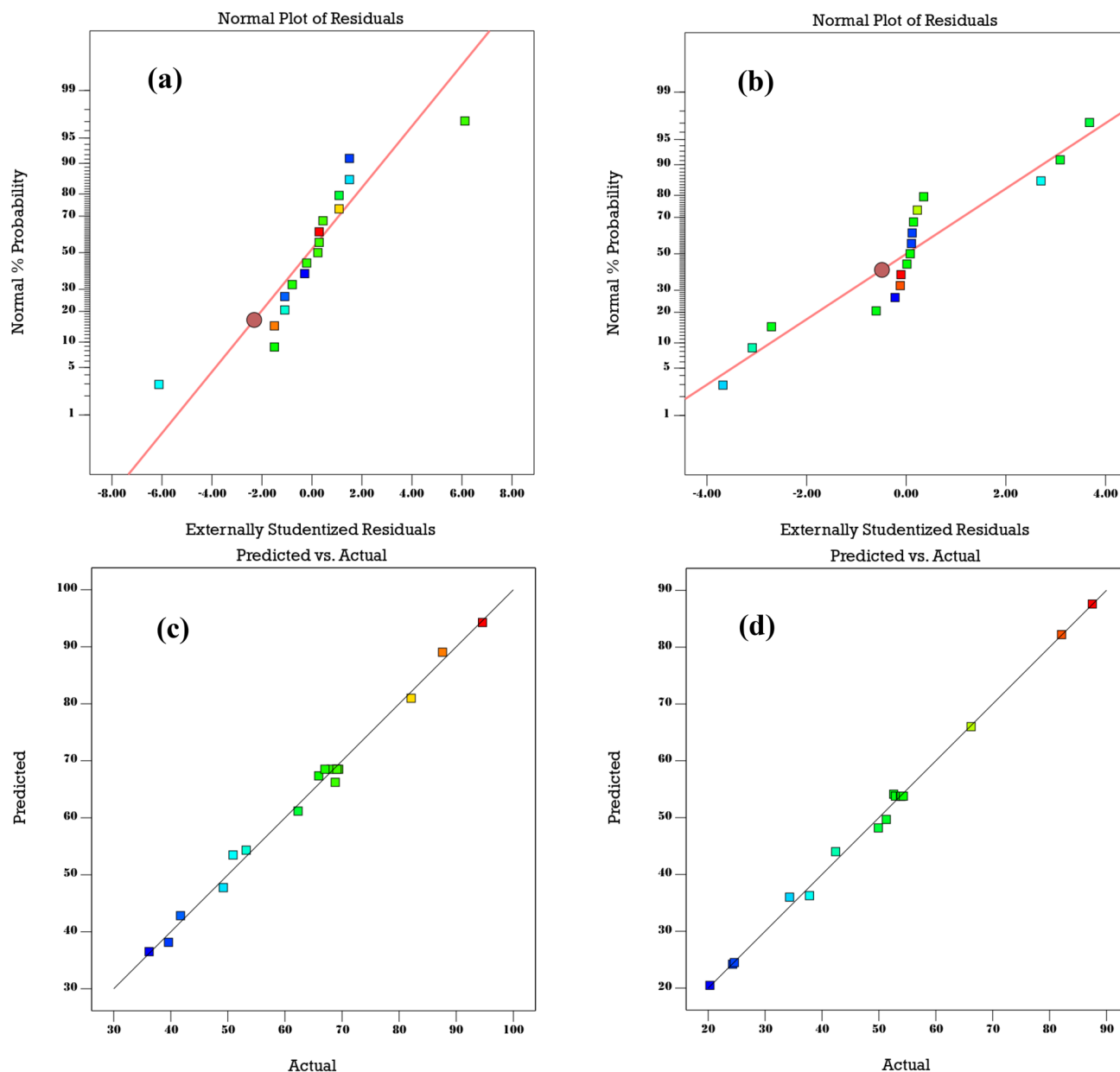


**Fig. 6** Normal probability plot of residuals for **a** RR4 removal by CS-ECH/TiO<sub>2</sub>-D and **b** RR4 removal by CS-ECH/TiO<sub>2</sub>-A; the plot of the relationship between the predicted and actual values of **c** RR4 removal by CS-ECH/TiO<sub>2</sub>-D, and **d** RR4 removal by CS-ECH/TiO<sub>2</sub>-A

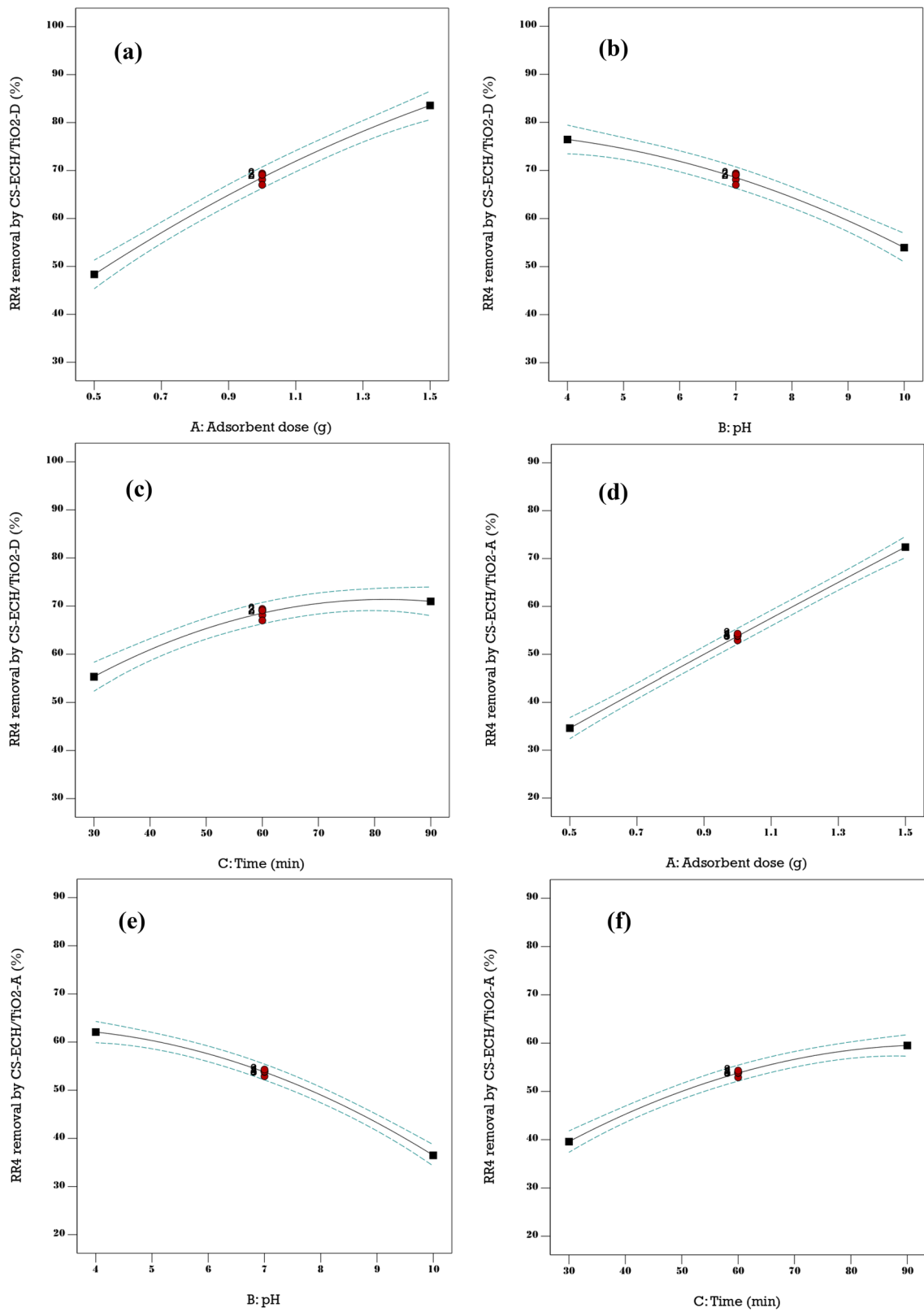


**Fig. 7** Plots of individual effects of **a** adsorbent dose, **b** pH, and **c** time factors on the RR4 removal by CS-ECH/TiO<sub>2</sub>-D, while **d** MAG dose, **e** pH, and **f** time are the individual effects of factors affecting the removal RR4 by CS-ECH/TiO<sub>2</sub>-A

a strong link between the practical responses (RR4 removal by CS-ECH/TiO<sub>2</sub>-D and RR4 removal by CS-ECH/TiO<sub>2</sub>-A) and those that are theoretically predicted, implying that the models are statistically credible [48].

### Effect of Individual Factors

The individual impacts of parameters influencing the RR4 dye adsorption process by CS-ECH/TiO<sub>2</sub>-D and CS-ECH/TiO<sub>2</sub>-A are illustrated in Fig. 7. At first, increasing the adsorbent dose (CS-ECH/TiO<sub>2</sub>-D or CS-ECH/TiO<sub>2</sub>-A) from 0.5 to 1.5 g leads to a reasonable increase in the removal (%)

of RR4 dye, as seen from Fig. 7a and d, respectively. This result is attributed to an increment in the number of binding sites (–NH<sub>2</sub> and –OH) and surface area (produced by TiO<sub>2</sub> particles) as the adsorbent dosage is increased. As shown in Fig. 7b and e, the pH factor contributes greatly to the removal of RR4 dye by CS-ECH/TiO<sub>2</sub>-D and CS-ECH/TiO<sub>2</sub>-A. As shown by Fig. 7b and e, the acidic medium is ideal for the removal of RR4 dye due to the extremely cationic sites of the adsorbent surface and the presence of negative charges in RR4 dye. Ultimately, as seen in Fig. 7c and f, the time factor seems to have an effective impact on the removal (%) of RR4 dye.

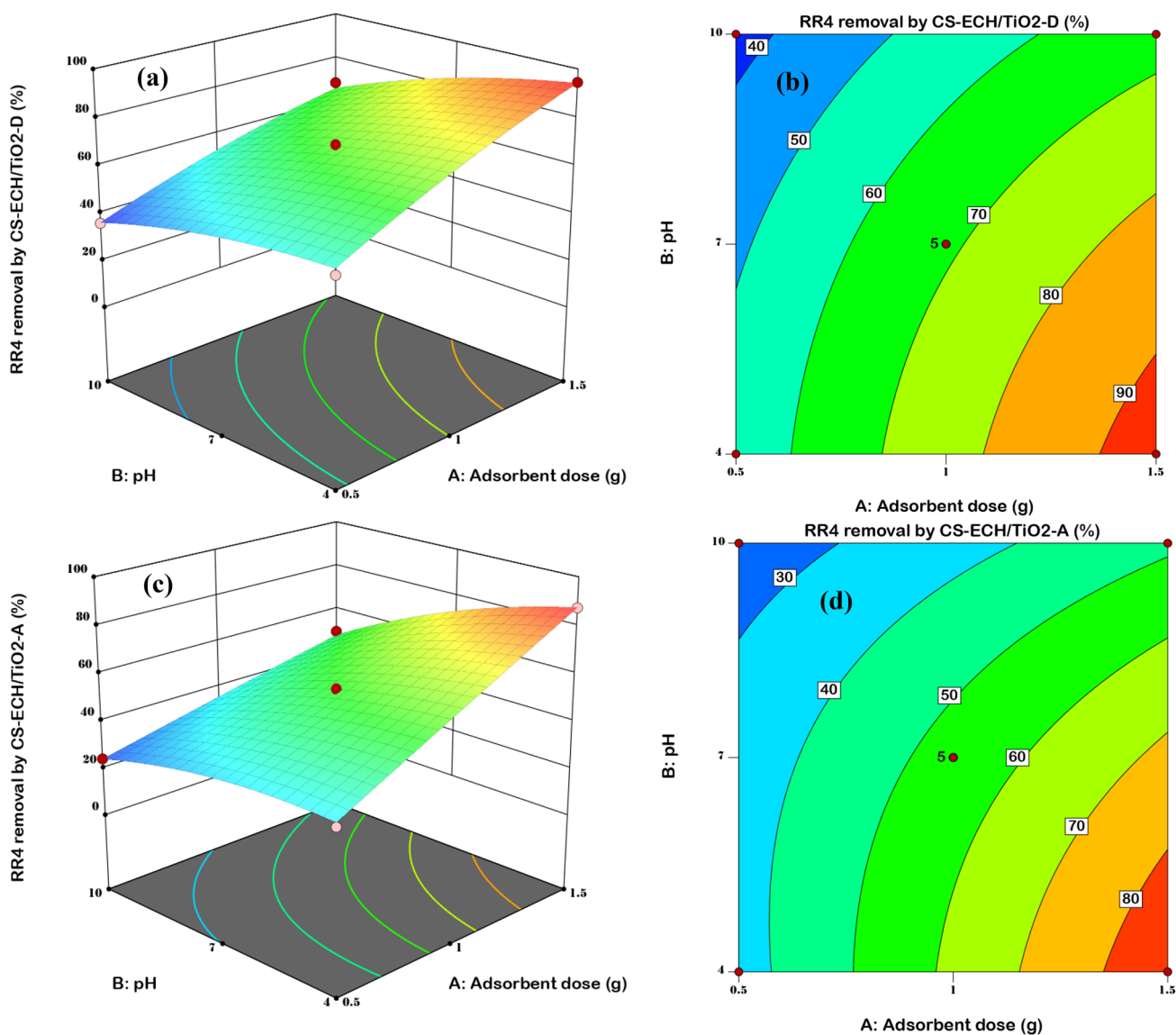
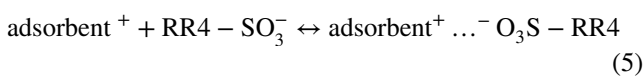


**Fig. 8** a 3D and b 2D plots of RR4 dye removal by CS-ECH/TiO<sub>2</sub>-D show interaction between adsorbent dose and pH; whereas, c 3D and d 2D plots of RR4 dye removal by CS-ECH/TiO<sub>2</sub>-A show interaction between adsorbent dose and pH

### Three-Dimensional (3D) Response Surfaces

3D surface and 2D contour plots were utilized to assess the influence of the studied variables and discover a relevant association between the analyzed variables affecting the RR4 dye removal process. Figure 8 demonstrates 3D and 2D diagrams of the critical association identified as AB (adsorbent dosage vs. pH) that influences the responses (RR4 removal by CS-ECH/TiO<sub>2</sub>-D and RR4 removal by CS-ECH/TiO<sub>2</sub>-A). The findings recorded in Fig. 8a–d demonstrate that the rising of CS-ECH/TiO<sub>2</sub>-(D/A) dose from 0.5 to 1.5 g improves the adsorption efficiency of RR4 dye. The increased RR4 dye adsorption rate is attributable to a significant number of functional groups (–OH<sub>2</sub><sup>+</sup>, –NH<sub>3</sub><sup>+</sup>, and Ti – OH<sub>2</sub><sup>+</sup>) on the surface of the CS-ECH/TiO<sub>2</sub>-(D/A) as well as the surface area caused by TiO<sub>2</sub> particles. These results are consistent with the FTIR results, which indicate that the CS-ECH/TiO<sub>2</sub>-(D/A) surfaces contain the aforementioned functional groups.

Additionally, as shown in Fig. 8a–d, the stepwise drop in pH value from 10 to 4 significantly increased the RR4 dye removal efficiency. To clarify the effect of pH on RR4 removal, two paths might be proposed: the p*H*<sub>pzc</sub> adsorbent property and the aimed form (cationic or anionic) of RR4 dye to attach on the surface of the adsorbent. The p*H*<sub>pzc</sub> values of CS-ECH/TiO<sub>2</sub>-D and CS-ECH/TiO<sub>2</sub>-A were 6.84 and 6.87, respectively. So, at high basic pH values, i.e. more than p*H*<sub>pzc</sub>, the adsorbent surface would be negatively charged. In contrast, in an extreme acidic medium (pH 4), i.e. pH < p*H*<sub>pzc</sub>, the adsorbent surface and RR4 dye molecules get positively and negatively charged, respectively. Therefore, at pH 4, the adsorbent's ability to bind the negatively charged RR4 dye molecules raises significantly, leading to enhancement in the adsorption process of RR4 dye, as shown in Eq. (5).



where adsorbent is either CS-ECH/TiO<sub>2</sub>-D or CS-ECH/TiO<sub>2</sub>-A.

Figure 9 gives 3D and 2D diagrams of the critical association identified as AC (adsorbent dosage vs. time) that influences the responses (RR4 removal by CS-ECH/TiO<sub>2</sub>-D and RR4 removal by CS-ECH/TiO<sub>2</sub>-A). The results outlined in Fig. 9a–d reveal that the rising of time from 30 to 90 min enhances the adsorption efficiency of RR4 dye. The high RR4 dye adsorption rate is due to the RR4 molecules needing enough time to diffuse into the inner pores of the CS-ECH/TiO<sub>2</sub>-(D/A) and to reach adsorption equilibrium.

### Adsorption Mechanism of RR4

FTIR examination indicated that the exterior composition of CS-ECH/TiO<sub>2</sub>-D and CS-ECH/TiO<sub>2</sub>-A is distinguished by a high content of powerful adsorption sites like hydroxyl (–OH), amino (–NH<sub>2</sub>), and Ti–OH groups, which is consistent with the literature [38, 42]. Due to the presence of these exceptional functional groups on the surface of CS-ECH/TiO<sub>2</sub>-D and CS-ECH/TiO<sub>2</sub>-A, it is a great candidate for the decolorization of hazardous dyes, especially anionic dyes. The adsorption mechanism for the RR4 acid dye on the surface of CS-ECH/TiO<sub>2</sub>-(D/A) was constructed based on the aforementioned as well as the FTIR and p*H*<sub>pzc</sub> investigations, as seen in Fig. 10. The critical interaction in the adsorption of RR4 dye is the electrostatic forces generated by the attraction between the positive charges on the surface of CS-ECH/TiO<sub>2</sub>-(D/A) formed from positively charged binding sites (–OH<sub>2</sub><sup>+</sup>, –NH<sub>3</sub><sup>+</sup>, and Ti – OH<sub>2</sub><sup>+</sup>) with the negative groups (–SO<sub>3</sub><sup>–</sup>) of RR4. Indeed, new kinds of hydroxyl groups have been added to the surface of CS-ECH/TiO<sub>2</sub>-(D/A) as a result of the loading of TiO<sub>2</sub> particles into the polymeric matrix of CS. Particularly in an acidic aqueous environment (pH 4), the terminal and bridging hydroxyl groups on the surface of CS-ECH/TiO<sub>2</sub>-(D/A) will be protonated and transformed into positive oxonium ions (–OH<sub>2</sub><sup>+</sup>). On the other hand, an aqueous solution can cause the sulfonate groups (–SO<sub>3</sub>H) of the RR4 to change into active negative sulfonate groups (–SO<sub>3</sub><sup>–</sup>). As a result, as seen in Fig. 10, a significant electrostatic interaction developed between the –SO<sub>3</sub><sup>–</sup> groups of RR4 and the –OH<sub>2</sub><sup>+</sup> ions on the surface of CS-ECH/TiO<sub>2</sub>-(D/A). Furthermore, hydrogen bonds serve an essential role in the adsorption mechanism because the presence of –NH<sub>2</sub> and –OH groups on the surface of CS-ECH/TiO<sub>2</sub>-(D/A) offers enough H to connect with the N and O atoms observed in the composition of RR4 dye. Lastly, n–π stacking offers an extra role in boosting adsorption ability, since these relationships arise from two phases, one being a nucleophile (groups having oxygen and nitrogen in the CS-ECH/TiO<sub>2</sub>-(D/A) and the second is an electrophile (benzene rings in RR4 dye) [49].

### Conclusion

Cross-linked chitosan composite was successfully modified with different TiO<sub>2</sub> phases (Degussa/Anatase) to attain efficient adsorbents (CS-ECH/TiO<sub>2</sub>-D and CS-ECH/TiO<sub>2</sub>-A) for the removal of reactive red 4 (RR4) dye from water. The highest removal derived from the BBD model of RR4 dye by CS-ECH/TiO<sub>2</sub>-D and RR4 removal by CS-ECH/TiO<sub>2</sub>-A

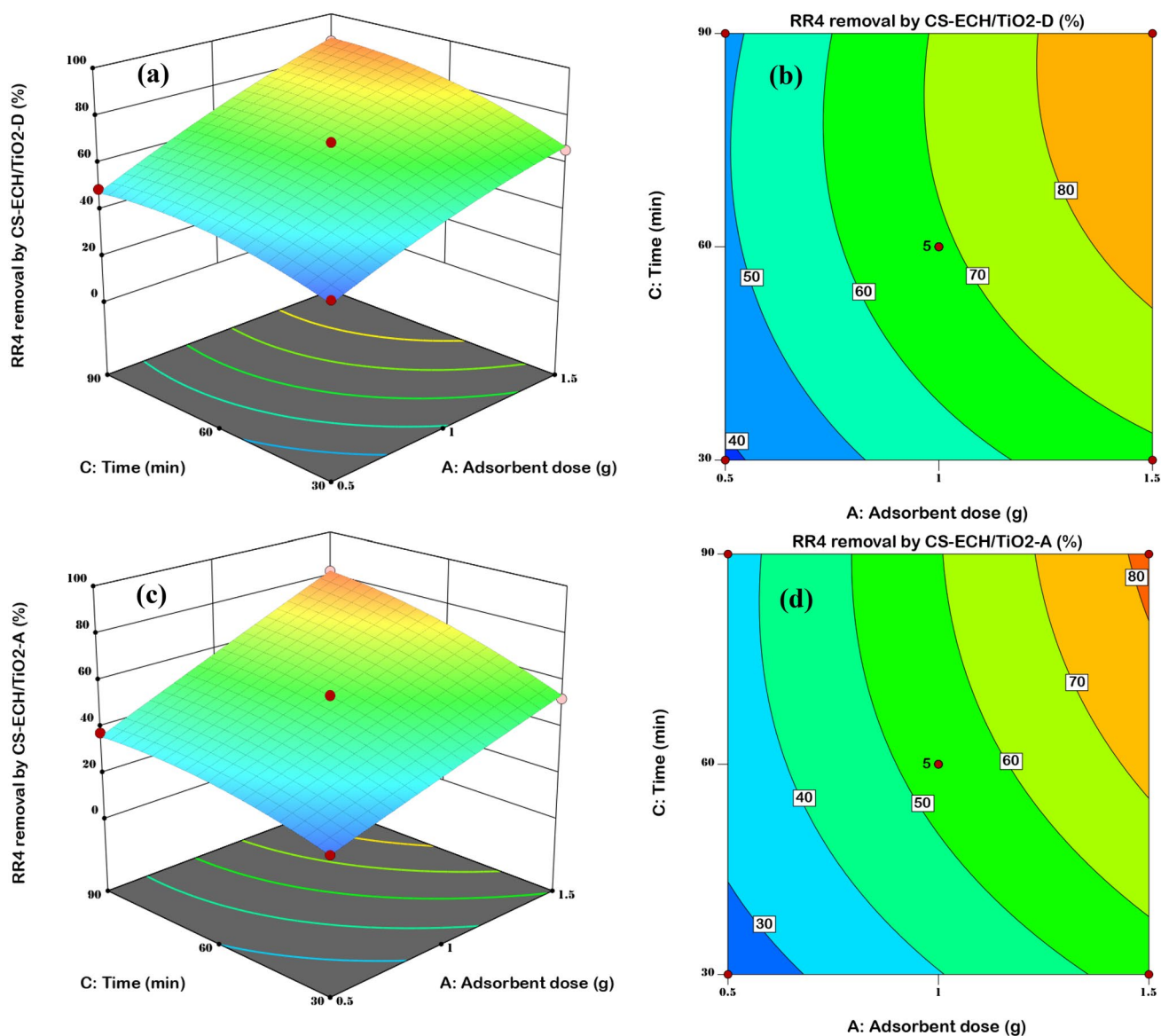


**Fig. 9** a 3D and b 2D plots of RR4 dye removal by CS-ECH/TiO<sub>2</sub>-D show the interaction between adsorbent dose and time; whereas, c 3D and d 2D plots of RR4 dye removal by CS-ECH/TiO<sub>2</sub>-A show interaction between adsorbent dose and time

was 94.6 and 87.5%, respectively. The high coefficient of determination ( $R^2 = 0.99$ ) value for both CS-ECH/TiO<sub>2</sub>-D and CS-ECH/TiO<sub>2</sub>-A suggested that the models were significant, and the chosen BBD was successful in improving RR4 dye removal. The best parameters for the maximum decoloration of RR4 dye based on the BBD model were adsorbent dosage = 1.5 g/L, pH 4, and the time = 60 min. The greatest decoloration of RR4 dye was attained at the

following vital interactions: AB (adsorbent dosage vs. initial pH) and AC (adsorbent dosage vs. time) interactions. The adsorption of RR4 molecules on the surface of CS-ECH/TiO<sub>2</sub> was constructed by many interactions e.g. electrostatic forces,  $n-\pi$  stacking, and H-bonding. This research reveals that CS-ECH/TiO<sub>2</sub>-D and CS-ECH/TiO<sub>2</sub>-A can be used as efficient bioadsorbents for the removal of acidic dyes from wastewater.

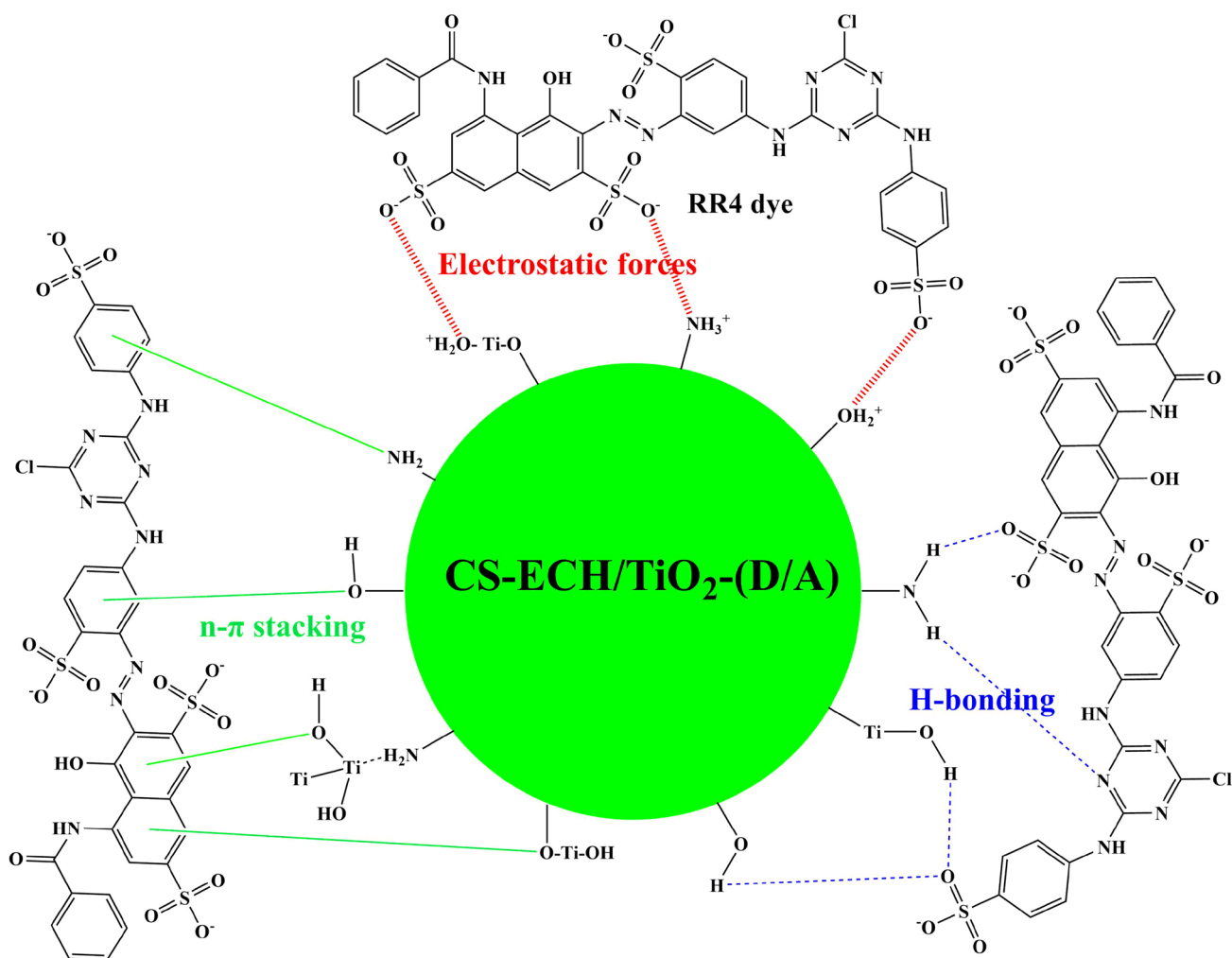


**Fig. 10** Illustration of the possible interaction between CS-ECH/TiO<sub>2</sub>-(D/A) surface and RR4 dye including electrostatic attraction, hydrogen bonding interactions, and n- $\pi$  interactions

**Acknowledgements** The authors would like to thank the Faculty of Applied Sciences, Universiti Teknologi MARA, Shah Alam for all facilities. The author (Zeid A. ALothman) is grateful to the Researchers Supporting Project No. (RSP-2021/1), King Saud University, Riyadh, Saudi Arabia.

**Author Contributions** All authors contributed to the study conception and design. Material preparation, data collection and analysis were performed by ASA, SV, AHJ, ZAA and ZMY. The first draft of the manuscript was written by ZMZ, ASA, AHJ and all authors commented on previous versions of the manuscript. All authors read and approved the final manuscript.

**Funding** Zeid A. ALothman has received research support from Researchers Supporting Project No. (RSP-2021/1), King Saud University, Riyadh, Saudi Arabia.

**Data Availability** The datasets generated during and/or analyzed during the current study are available from the corresponding author on reasonable request.

## Declarations

**Competing interest** The authors have no relevant financial or non-financial interests to disclose.

## References

- Rathi BS, Kumar PS, Vo DVN (2021) Critical review on hazardous pollutants in water environment: occurrence, monitoring, fate, removal technologies and risk assessment. *Sci Total Environ* 797:149134
- Azami MS, Ismail K, Ishak MAM, Zuliahani A, Hamzah SR, Nawawi WI (2020) Formation of an amorphous carbon nitride/titania composite for photocatalytic degradation of RR4 dye. *J Water Process Eng* 35:101209
- Abd Malek NN, Yousif E, Jawad EAH (2020) Optimization of adsorption parameters for reactive red 4 (RR4) removal by cross-linked chitosan-epichlorohydrin using Box Behnken design. *Sci Lett* 14(1):83–95

4. Xiang J, Li H, Hei Y, Tian G, Zhang L, Cheng P, Tang N (2022) Preparation of highly permeable electropositive nanofiltration membranes using quaternized polyethyleneimine for dye wastewater treatment. *J Water Process Eng* 48:102831
5. Shao D, Wang Z, Zhang C, Li W, Xu H, Tan G, Yan W (2022) Embedding wasted hairs in Ti/PbO<sub>2</sub> anode for efficient and sustainable electrochemical oxidation of organic wastewater. *Chin Chem Lett* 33(3):1288–1292
6. de Almeida EJR, Mazzeo DEC, Sommaggio LRD, Marin-Morales MA, de Andrade AR, Corso CR (2019) Azo dyes degradation and mutagenicity evaluation with a combination of microbiological and oxidative discoloration treatments. *Ecotoxicol Environ Safe* 183:109484
7. Rafea HAG, Yusop NFM, Azmi NF, Abdullah NS, Ramli NIT (2021) Photocatalytic degradation of methylene blue dye solution using different amount of ZnO as a photocatalyst. *Sci Lett* 15(1):1–12
8. Muthukumar P, Sowmiya E, Arunkumar G, Pannipara M, Al-Sehemi AG, Anthony SP (2022) Highly enhanced dye adsorption of MoO<sub>3</sub> nanoplates fabricated by hydrothermal-calcination approach in presence of chitosan and thiourea. *Chemosphere* 291:132926
9. Jawad AH, Abdulhameed AS, Bahrudin NN, Hum NNMF, Surip SN, Syed-Hassan SSA, Sabar S (2021) Microporous activated carbon developed from KOH activated biomass waste: surface mechanistic study of methylene blue dye adsorption. *Water Sci Technol* 84(8):1858–1872
10. Shoueir KR, El-Desouky N, Rashad MM, Ahmed MK, Janowska I, El-Kemary M (2021) Chitosan based-nanoparticles and nanocapsules: overview, physicochemical features, applications of a nanofibrous scaffold, and bioprinting. *Int J Biol Macromol* 167:1176–1197
11. Jawad AH, Abdulhameed AS, Wilson LD, Hanafiah MAKM, Nawawi WI, ALOthman ZA, Rizwan Khan M (2021) Fabrication of schiff's base chitosan-glutaraldehyde/activated charcoal composite for cationic dye removal: optimization using response surface methodology. *J Polym Environ* 29(9):855–2868
12. Omer AM, Dey R, Eltaweil AS, El-Monaem AEM, Ziora ZM (2022) Insights into recent advances of chitosan-based adsorbents for sustainable removal of heavy metals and anions. *Arab J Chem* 15(2):103543
13. Motaghi H, Arabkhani P, Parvinnia M, Asfaram A (2021) Simultaneous adsorption of cobalt ions, azo dye, and imidacloprid pesticide on the magnetic chitosan/activated carbon@ UiO-66 bio-nanocomposite: optimization, mechanisms, regeneration, and application. *Sep Pur Technol* 284:120258
14. Farrokhi Z, Sadjadi S, Raouf F, Bahri-Laleh N (2022) Novel bio-based Pd/chitosan-perlite composite bead as an efficient catalyst for rapid decolorization of azo dye. *Inorg Chem Commun* 143:109734
15. Rajendiran R, Patchaiyappan A, Harisingh S, Balla P, Paari A, Ponnala B, Seelam PK (2022) Synergistic effects of graphene oxide grafted chitosan & decorated MnO<sub>2</sub> nanorods composite materials application in efficient removal of toxic industrial dyes. *J Water Process Eng* 47:102704
16. Zhao X, Wang X, Lou T (2022) Simultaneous adsorption for cationic and anionic dyes using chitosan/electrospun sodium alginate nanofiber composite sponges. *Carbohydr Polym* 276:118728
17. Khapre MA, Pandey S, Jugade RM (2021) Glutaraldehyde-cross-linked chitosan–alginate composite for organic dyes removal from aqueous solutions. *Int J Biol Macromol* 190:862–875
18. Zubair M, Aziz HA, Ihsanullah I, Ahmad MA, Al-Harathi MA (2022) Enhanced removal of eriochrome black T from water using biochar/layered double hydroxide/chitosan hybrid composite: performance evaluation and optimization using BBD-RSM approach. *Environ Res* 209:112861
19. Wang F, Li L, Iqbal J, Yang Z, Du Y (2022) Preparation of magnetic chitosan corn straw biochar and its application in adsorption of amaranth dye in aqueous solution. *Int J Biol Macromol* 199:234–242
20. Jawad AH, Abdulhameed AS, Kashi E, Yaseen ZM, ALOthman ZA, Khan MR (2022) Cross-linked chitosan-glyoxal/kaolin clay composite: parametric optimization for color removal and COD reduction of remazol brilliant blue R dye. *J Polym Environ* 30(1):164–178
21. Şenol ZM, Çetinkaya S, Yenidünya AF, Başoğlu-Ünal F, Ece A (2022) Epichlorohydrin and tripolyphosphate-crosslinked chitosan–kaolin composite for auramine O dye removal from aqueous solutions: experimental study and DFT calculations. *Int J Biol Macromol* 199:318–330
22. Li Y, Liang YQ, Mao XM, Li H (2022) Efficient removal of Cu (II) from an aqueous solution using a novel chitosan assisted EDTA-intercalated hydrotalcite-like compound composite: preparation, characterization, and adsorption mechanism. *Chem Eng J* 438:135531
23. Hermosillo-Ochoa E, Picos-Corralles LA, Licea-Claverie A (2021) Eco-friendly flocculants from chitosan grafted with PNVCL and PAAc: hybrid materials with enhanced removal properties for water remediation. *Sep Pur Technol* 258:118052
24. Raval NP, Mukherjee S, Shah NK, Gikas P, Kumar M (2021) Hexametaphosphate cross-linked chitosan beads for the eco-efficient removal of organic dyes: tackling water quality. *J Environ Manage* 280:111680
25. Jawad AH, Abdulhameed AS, Mastuli MS (2020) Mesoporous crosslinked chitosan-activated charcoal composite for the removal of thionine cationic dye: comprehensive adsorption and mechanism study. *J Polym Environ* 28(3):1095–1105
26. Billah REK, Shekhawat A, Mansouri S, Majdoubi H, Agunaou M, Soufiane A, Jugade R (2022) Adsorptive removal of Cr (VI) by Chitosan–SiO<sub>2</sub>–TiO<sub>2</sub> nanocomposite. *Environ Nanotechnol Monit Manage* 18:100695
27. Jawad AH, Abdulhameed AS, Selvasembian R, ALOthman ZA, Wilson LD (2022) Magnetic biohybrid chitosan-ethylene glycol diglycidyl ether/magnesium oxide/Fe<sub>3</sub>O<sub>4</sub> nanocomposite for textile dye removal: Box–Behnken design optimization and mechanism study. *J Polym Res* 29(5):1–15
28. Mubarak NSA, Sabar S, Jawad AH (2020) The study of commercial titanium dioxide (TiO<sub>2</sub>) Degussa P25 for the adsorption of acidic dye. *Sci Lett* 14:68–83
29. de Menezes FLG, de Lima Leite RH, dos Santos FKG, Aria AI, Aroucha EMM (2021) TiO<sub>2</sub>-enhanced chitosan/cassava starch biofilms for sustainable food packaging. *Colloids Surf A* 630:127661
30. Shehzad H, Ahmed E, Sharif A, Farooqi ZH, Din MI, Begum R, Nawaz I (2022) Modified alginate-chitosan-TiO<sub>2</sub> composites for adsorptive removal of Ni (II) ions from aqueous medium. *Int Biol Macromol* 194:117–127
31. Cui HF, Zhang TT, Lv QY, Song X, Zhai XJ, Wang GG (2019) An acetylcholinesterase biosensor based on doping Au nanorod@ SiO<sub>2</sub> nanoparticles into TiO<sub>2</sub>-chitosan hydrogel for detection of organophosphate pesticides. *Biosens Bioelect* 141:111452
32. Rahmanpour A, Farahpour MR, Shapouri R, Jafarirad S, Rahimi P (2022) Synthesis and characterization of alumina-based nanocomposites of TiO<sub>2</sub>/Al<sub>2</sub>O<sub>3</sub>/Chitosan with antibacterial properties accelerate healing of infected excision wounds. *Colloids Surf A* 644:128839
33. Dalvand A, Nabizadeh R, Ganjali MR, Khoobi M, Nazmara S, Mahvi AH (2016) Modeling of reactive blue 19 azo dye removal from colored textile wastewater using L-arginine-functionalized

- Fe<sub>3</sub>O<sub>4</sub> nanoparticles: optimization, reusability, kinetic and equilibrium studies. *J Magnet Magnet Mater* 404:179–189
34. Sing KS (1985) Reporting physisorption data for gas/solid systems with special reference to the determination of surface area and porosity (Recommendations 1984). *Pure Appl Chem* 57(4):603–619
  35. Lin J, Zhan Y (2012) Adsorption of humic acid from aqueous solution onto unmodified and surfactant-modified chitosan/zeolite composites. *Chem Eng J* 200:202–213
  36. Jbeli A, Hamden Z, Bouattour S, Ferrara AM, Conceição DS, Ferreira LV, Boufi S (2018) Chitosan-Ag-TiO<sub>2</sub> films: an effective photocatalyst under visible light. *Carbohydr Polym* 199:31–40
  37. Hussein EM, Desoky WM, Hanafy MF, Guirguis OW (2021) Effect of TiO<sub>2</sub> nanoparticles on the structural configurations and thermal, mechanical, and optical properties of chitosan/TiO<sub>2</sub> nanoparticle composites. *J Phys Chem Sol* 152:109983
  38. Jawad AH, Mubarak NSA, Abdulhameed AS (2020) Hybrid crosslinked chitosan-epichlorohydrin/TiO<sub>2</sub> nanocomposite for reactive red 120 dye adsorption: kinetic, isotherm, thermodynamic, and mechanism study. *J Polym Environ* 28(2):624–637
  39. Kamari Y, Ghiaci M (2016) Preparation and characterization of ibuprofen/modified chitosan/TiO<sub>2</sub> hybrid composite as a controlled drug-delivery system. *Micropor Mesopor Mater* 234:361–369
  40. Tao Y, Pan J, Yan S, Tang B, Zhu L (2007) Tensile strength optimization and characterization of chitosan/TiO<sub>2</sub> hybrid film. *Mater Sci Eng* 138(1):84–89
  41. Yang D, Li J, Jiang Z, Lu L, Chen X (2009) Chitosan/TiO<sub>2</sub> nanocomposite pervaporation membranes for ethanol dehydration. *Chem Eng Sci* 64(13):3130–3137
  42. Anaya-Esparza LM, Ruvalcaba-Gómez JM, Maytorena-Verdugo CI, González-Silva N, Romero-Toledo R, Aguilera-Aguirre S, Montalvo-González E (2020) Chitosan-TiO<sub>2</sub>: a versatile hybrid composite. *Mater* 13(4):811
  43. Jawad AH, Abdulhameed AS, Kashi E, Yaseen ZM, Alothman ZA, Khan MR (2022) Cross-linked chitosan-glyoxal/kaolin clay composite: parametric optimization for color removal and COD reduction of remazol brilliant blue R dye. *J Polym Environ* 30(1):164–178
  44. Cheng Z, Zhang L, Guo X, Jiang X, Liu R (2015) Removal of lissamine rhodamine B and acid orange 10 from aqueous solution using activated carbon/surfactant: process optimization, kinetics and equilibrium. *J Taiwan Inst Chem Eng* 47:149–159
  45. Alhalili Z (2022) Green synthesis of copper oxide nanoparticles CuO NPs from *Eucalyptus globoulus* leaf extract: adsorption and design of experiments. *Arab J Chem* 15(5):103739
  46. Rumjit NP, Samsudin NA, Low FW, Thomas P, Lai CW, Chellam PV, Tiong SK (2021) Kinetic and isotherm studies on adsorptive removal of sulfates by cotton shell derived biochar: recovery of sulfates from marcasite soil. *Sustain Chem Pharm* 20:100361
  47. Samal K, Dash RR (2021) Modelling of pollutants removal in integrated vermifilter (IVmF) using response surface methodology. *Clean Eng Technol* 2:100060
  48. Lacson CFZ, Lu MC, Huang YH (2022) Calcium-based seeded precipitation for simultaneous removal of fluoride and phosphate: its optimization using BBD-RSM and defluoridation mechanism. *J Water Process Eng* 47:102658
  49. Singh SK, Das A (2015) The  $n \rightarrow \pi^*$  interaction: a rapidly emerging non-covalent interaction. *Phys Chem Chem Phys* 17(15):9596–9612

**Publisher's Note** Springer Nature remains neutral with regard to jurisdictional claims in published maps and institutional affiliations.

Springer Nature or its licensor holds exclusive rights to this article under a publishing agreement with the author(s) or other rightsholder(s); author self-archiving of the accepted manuscript version of this article is solely governed by the terms of such publishing agreement and applicable law.